Pergamon

Int. J. Heat Mass Transfer. Vol. 39, No. 2, pp. 391–405, 1996

0017-9310/96 $9.50+0.00

0017-9310(95)00113-1

Heat transfer, condensation and fog formation in crossflow plastic heat exchangers

H. J. H. BROUWERS†

Akzo Nobel Central Research Arnhem, Fibres Division, Department of Mechanical Engineering, Velperweg 76, 6824 BM Arnhem, The Netherlands

and

C. W. M. VAN DER GELD

Eindhoven University of Technology, Department of Mechanical Engineering, P.O. Box 513, 5600 MB Eindhoven, The Netherlands

(*Received* 18 *October* 1994)

Abstract—In this paper heat transfer of air–water-vapour mixtures in plastic crossflow heat exchangers is studied theoretically and experimentally. First, a model for heat transfer without condensation is derived, resulting in a set of classical differential equations. Subsequently, heat transfer with wall condensation and fog formation are considered in some detail. Separate attention is paid to the heat transfer and condensation of pure steam in the heat exchanger. Finally, the experiments performed are reported and the results compared with the models presented. From this comparison it can be learnt that the models are well able to predict the rate of heat transfer and phenomena such as condensation and fog formation.

INTRODUCTION

The present research was dictated by the need to develop a numerical model of plastic gas–liquid compact heat exchangers, as depicted in Fig. 1. These crossflow heat exchangers have been developed at Akzo Nobel's research institute and are made entirely from polyvinylidene fluoride (PVDF) or polypropylene (PP). The heat exchangers consist of plates containing small channels and hence possess only primary, or direct, heat transfer surfaces. The use of plastic as the material permits the heat exchangers to be used for heat recovery from sometimes corrosive process gases. Condensable components in the gas, such as water-vapour, sulphur oxides and nitrogen oxides, may form condensate films along the corrosion-resistant walls. The maximum operational temperatures of the PP and PVDF heat exchangers—when properly cooled—are limited to 100 and 200°C, respectively.

As the costs of the heat exchangers are directly related to the heat exchanging surface area, there is a need to determine the required heat transfer surface as accurately as possible. The rating of a heat exchanger is adapted to the specific process requirements of the customer. As such, dimensioning is preferably performed on the customer's premises, and the calculation should be executable on a portable personal computer (PC). Yet, the modelling should be based on reliable expressions for heat and mass transfer, taking into account the special features of plastic heat exchangers.

The gas and liquid flows entering the heat exchanger spread approximately equally over the various channels of the heat exchanger. This allows the analysis to be limited to the consideration of one plate. Figure 1 reveals that the transfer between the fluids is a three-dimensional process; the physical properties vary in the direction of both fluid flows and also across the channels. However, employing the mean mixed values (i.e. the values that would result after mixing of the flow across a channel) of temperatures and water-vapour mass fraction, the modelling problem becomes two-dimensional. For the simplest case, heat transfer without condensation on the gas side, this approach results in a set of differential equations whose solution is well documented in the literature. This case is presented first.

Subsequently, the equations of partial and pure water-vapour condensation are formulated, taking superheating and large vapour mass fractions into account. In the case of partial vapour condensation the temperature of the condensate–gas interface is not known explicitly, and is furthermore non-uniform. For pure vapour condensation this temperature is known, being equal to the saturation temperature of the vapour, but here the vapour mass flux to the condensate is unknown. In both cases, however, the unknown quantity follows from a local energy balance

† Present address: University of Twente, Department of Civil Engineering and Management, P.O. Box 217, 7500 AE Enschede, The Netherlands.

NOMENCLATURE

B	net plate width [m]
c	vapour mass fraction
c_p	specific heat [J kg^{-1} K^{-1}]
$\mathbb{D}$	diffusion coefficient [m^2 s^{-1}]
D_h	hydraulic diameter; four times the cross-sectional area/the perimeter [m]
d_i	geometrical property of heat exchanger, see Fig. 2 [m]
F	saturation function
g	acceleration due to gravity [m s^{-2}]
g_m	mass transfer coefficient [kg m^{-2} s^{-1}]
h	heat transfer coefficient [W m^{-2} K^{-1}]
H_{lat}	latent heat of condensation [J kg^{-1}]
k	thermal conductivity [W m^{-1} K^{-1}]
L	net plate length [m]
Le	Lewis number, $k/\rho c_p\mathbb{D}$
Le_v	modified Lewis number, $k/\rho c_{p,v}\mathbb{D}$
$\dot{m}$	mass flux to wall [kg m^{-2} s^{-1}]
$\dot{m}_f$	bulk fog, equation (27) [kg m^{-2} s^{-1}]
NTU	number of transfer units, defined by equations (9) or (10)
Nu	Nusselt number, hD_h/k
P	pressure [bar]
RH	relative humidity
Re_g	gas Reynolds number, $2w_{g,in}/L\eta$
Re_l	liquid Reynolds number, $w_l/B\eta_l$
Sh	Sherwood number, $g_mD_h/\rho\mathbb{D}$
t	temperature [°C]
w	mass flow rate [kg s^{-1}]
W	dimensionless mass flow rate, sec equation (37)
x	coordinate in direction of gas flow [m]
X	dimensionless coordinate, $X = x/B$
z	coordinate in direction of liquid flow [m]
Z	dimensionless coordinate, $Z = x/L$.

Greek symbols

ζ	dimensionless temperature, defined by equations (36)
η	dynamic viscosity [Pa s]
Θ	correction factor
ρ	density [kg m^{-3}]
ϕ_t	dimensionless wall mass flux, $\dot{m}c_{p,v}/\bar{h}_g$.

Subscripts

c	diffusional
con	condensate
dew	dew point
f	fog
g	gas mixture
i	channel plate/gas or condensate/gas interface
in	entry
l	liquid in channel plate
out	exit
pl	channel plate
sat	saturation
t	thermal
tot	total
v	vapour
w	channel plate wall.

Superscripts

inv	inverse
¯	mean mixed or 'bulk'.

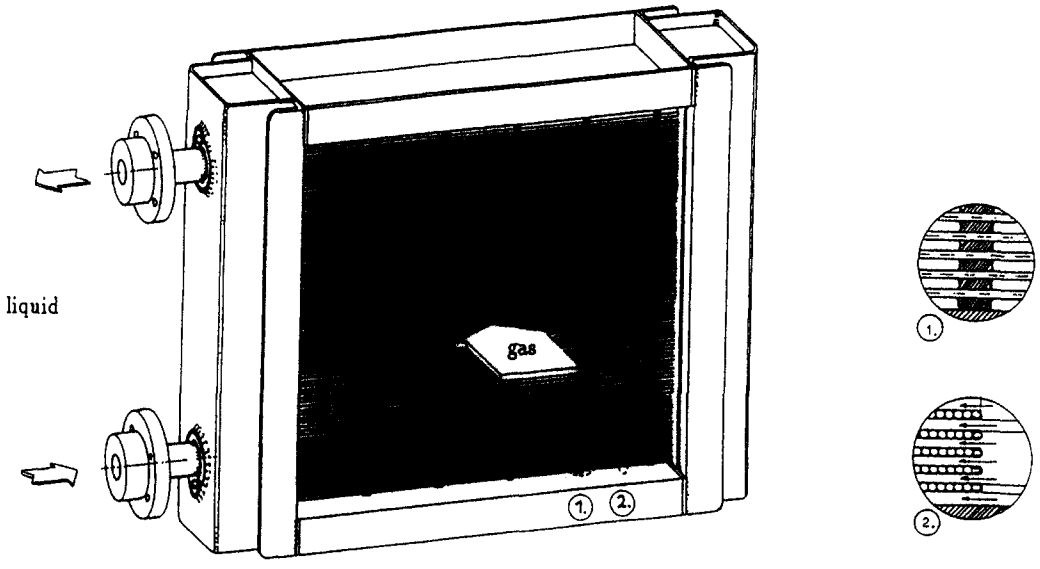

Fig. 1. The plastic heat exchanger. (1) View in the direction of gas flow. (2) View in the direction of liquid flow.

of heat fluxes to and from the condensate surface. A second complication when condensation occurs is that the heat and mass transfer on the gas side is enhanced by the transport of vapour (corresponding, effectively, to 'suction' through a porous boundary). In this paper the classical film model is adopted to account for this effect, since it provides local correction factors for the transfer rates and simple first order differential equations for the decrement in temperature, mass flow rate and pressure in a closed channel. In the past this one-dimensional model, which neglects convective and diffusive transport in the direction of flow, has proved satisfactory in many practical applications. Reviews of this model are found in refs. [1–4].

Exploratory computations of heat transfer from mixtures of non-condensables and water-vapour reveal that the mixed mean water-vapour fraction and temperature of the gas mixture may correspond to supersaturation, so that fog is likely to be formed in the gas flow. Fog formation alters heat and mass transfer rates from gas to wall and hence the performance of the heat exchanger. Moreover, the occurrence and rate of fog formation are of utmost importance. In processes aimed solely at heat recovery it is an undesirable phenomenon since the droplets formed represent a yield loss and are difficult to remove. For gas washing applications, however, both the droplets and condensate films are very well suited to absorb toxic and/or corrosive gas components (implying that the heat exchanger should be used in combination with a fog removal device). Accordingly, both of the fog film models of Brouwers [5, 6] are employed to account for the effects of both suction and fog formation.

Some performance characteristics of the heat exchanger are illustrated by application of the models to various mixtures of air and water-vapour. The theoretical predictions are compared with experiments, carried out with a PVDF heat exchanger placed in a wind tunnel, to verify the models presented in this paper.

HEAT TRANSFER WITHOUT CONDENSATION

In this section the heat transfer between gas and liquid is discussed without any condensation at the gas side. Condensation will not take place when the gas is heated in the heat exchanger, or when the gas is cooled and the coldest spot in the heat exchanger is hotter than the dew point of the mixture or saturation temperature of pure vapour. The exact condition for condensation in terms of the inlet conditions will be specified at the end of this section.

The gas flows between the channel plates in the X direction and the liquid through the plates in the Z direction (see Fig. 2). Both flows are laminar under standard operating conditions, their Reynolds number ranging from 200 to 2000. The coordinates X and Z are rendered dimensionless by means of the net width B and length L of the plate, respectively. The net effective width of the plate B relates to the total width B_{tot} minus the thickness of a partition wall times the number of coolant channels, see Figs. 1(2) and 2. The net length L is formed by the total length of the plate minus the total length taken up by the intermediate reinforcements of the plates, see Fig. 1(1). In Fig. 1 one can see that their relative distance is of magnitude B_{tot}. The different gas and liquid temperatures cause sensible heat transfer, and an energy balance for an element $dX\,dZ$ yields:

$$\bar{h}_g(\bar{t}_g - t_i) = \bar{h}_{pl}(t_i - \bar{t}_l). \tag{1}$$

Here $\bar{t}_g(X, Z)$ and $\bar{t}_l(X, Z)$ represent the mixed mean temperatures of gas and liquid, respectively. All (physical) properties of the gas are assigned the subscript 'g' to distinguish them from the liquid properties, which are assigned the subscript 'l'. By making use of the mixed mean temperatures the three-dimensional process in the heat exchanger is simplified to a two-dimensional model.

The heat transfer coefficient $\bar{h}_g$ from gas to wall, which turns out to be about 55 W m^{-2} K^{-1}, can be found in ref. [3]: the mean heat transfer coefficient $\bar{h}_{pl}$ of the plate consists of two parts:

$$\frac{1}{\bar{h}_{pl}} = \frac{1}{\bar{h}_w} + \frac{1}{\bar{h}_l}. \tag{2}$$

The mean heat transfer coefficient $\bar{h}_w$ of the plate proves to be about 950 W m^{-2} K^{-1} and the mean heat transfer coefficient $\bar{h}_l$ from wall to liquid has a value of at least 1500 W m^{-2} K^{-1} [3].

The heat exchange yields an alteration of the bulk gas and liquid temperatures. For the liquid the differential energy balance relation reads:

$$\frac{w_l c_{p,l}}{BL}\frac{\partial \bar{t}_l}{\partial Z} = 2\bar{h}_{pl}(t_i - \bar{t}_l) \tag{3}$$

subject to the boundary condition:

$$\bar{t}_l(X, Z = 0) = t_{l,in}. \tag{4}$$

For the gas:

$$\frac{w_g c_{p,g}}{BL}\frac{\partial \bar{t}_g}{\partial X} = 2\bar{h}_g(t_i - \bar{t}_g) \tag{5}$$

with the associated boundary condition:

$$\bar{t}_g(X = 0, Z) = t_{g,in}. \tag{6}$$

The factor of two in equations (3) and (5) takes into account the heat transfer at both sides of the plate. The mass flow rate through a single gas channel is given by the total gas mass flow rate divided by the number of plates. The liquid mass flow rate per plate is equal to the total liquid mass flow rate divided by the number of channel plates, times the number of times the liquid passes the heat exchanger. In Fig. 1 the example of a heat exchanger with two liquid passes is depicted. Equation (1) is now rewritten, yielding t_i as a combination of $\bar{t}_g$ and $\bar{t}_l$. The result is substituted in equations (3) and (5), yielding:

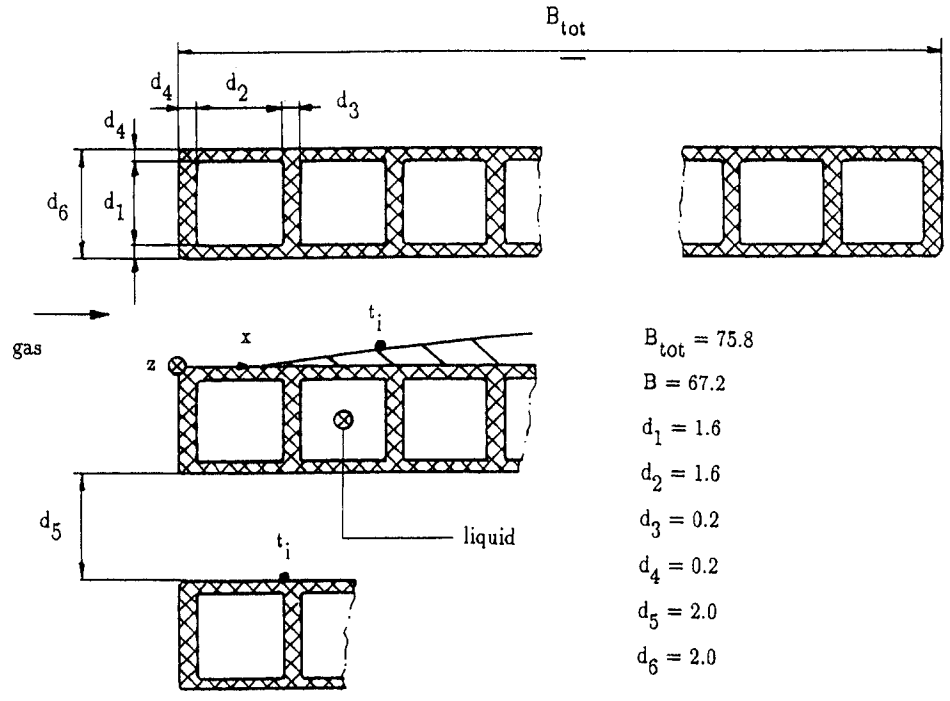

Fig. 2. Heat transfer between channel plates (sizes in millimetres).

$$\frac{\partial \bar{t}_l}{\partial Z} = NTU_l(\bar{t}_g - \bar{t}_l) \tag{7}$$

$$\frac{\partial \bar{t}_g}{\partial X} = NTU_g(\bar{t}_l - \bar{t}_g). \tag{8}$$

In these equations the number of transfer units are introduced as:

$$NTU_l = \frac{2\bar{h}_{tot}LB}{w_l c_{p,l}} \tag{9}$$

$$NTU_g = \frac{2\bar{h}_{tot}LB}{w_g c_{p,g}}. \tag{10}$$

The mean total heat transfer coefficient $\bar{h}_{tot}$ from gas to liquid is defined by:

$$\frac{1}{\bar{h}_{tot}} = \frac{1}{\bar{h}_{pl}} + \frac{1}{\bar{h}_g} = \frac{1}{\bar{h}_w} + \frac{1}{\bar{h}_l} + \frac{1}{\bar{h}_g} \tag{11}$$

[see equation (2)]. In order to find out whether condensation takes place on the plates at the gas side, the minimum plate surface temperature $t_i(1,0)$ is determined. Equation (8), combined with equations (4) and (6), is solved at $Z = 0$. The result is substituted into equation (1) and equation (11) applied, yielding as the minimum surface temperature:

$$t_i(X = 1, Z = 0) = t_{l,in} + (t_{g,in} - t_{l,in})\frac{\bar{h}_{tot}}{\bar{h}_{pl}} e^{-NTU_g}. \tag{12}$$

Water will not condense if the temperature of this coldest spot on the plate is higher than the saturation temperature of pure steam or the dew point temperature of a mixture.

The solution of the coupled equations (7) and (8), with boundary conditions (4) and (6), depends only on both numbers of transfer units. These crossflow equations have been solved by many investigators, starting with Nusselt [7]. In the letter of Baclic and Heggs [8] a broad review is presented of all treatments and equivalent solutions of these classical equations. Here the solution of Mason [9] is used from which the mixed mean exit temperature of the liquid, defined as:

$$t_{l,out} = \bar{t}_l(Z = 1) = \int_{X=0}^{1} \bar{t}_l(X, Z = 1)\,dX \tag{13}$$

is obtained. As mass is not extracted, the gas mass flow rate at the end of the gap is evidently equal to the entry gas mass flow rate. Accordingly, the mean exit gas temperature then readily follows from an overall energy balance. In a heat exchanger in which the liquid passes more than one time, e.g. see Fig. 1, the heat transfer of each pass has to be calculated in the manner described here. The exit temperature of a pass serves as entry temperature of the following pass, until the liquid leaves the last pass and heat exchanger. The mixed mean exit gas temperature follows from the arithmetic mean of the determined exit gas temperatures of each pass.

PARTIAL WATER-VAPOUR CONDENSATION (AND FOG FORMATION)

In this section the partial condensation of water-vapour (or steam) in the presence of non-con-

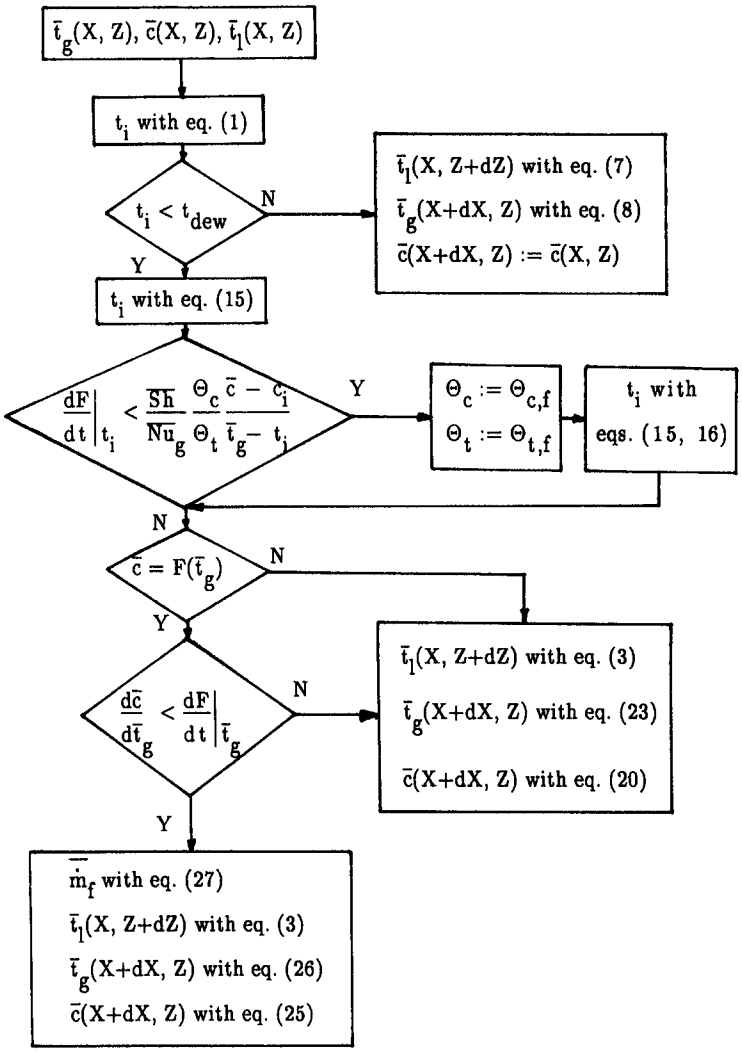

Fig. 3. Flow chart of calculational procedure for partial water-vapour condensation.

densables is modelled, accounting for the possible formation of fog. The equations governing heat and mass transfer due to temperature and concentration differences between gas and condensate surface are derived and solved numerically. The followed procedure is illustrated by means of the flow chart in Fig. 3.

Using equation (12) it is verified whether condensation takes place. When water-vapour condenses on the coldest spot on the plates, it is likely to condense at some other locations as well. This is examined by calculating the local interface temperature $t_i(X, Z)$ by means of equation (1), thus assuming *a priori* that there is no condensation. If no condensation takes place than the governing equations (7) and (8) hold locally. On the other hand, condensation takes place if:

$$t_i > t_{dew} = F^{inv}(\bar{c}) \tag{14}$$

where $\bar{c}(X, Z)$ denotes the local bulk vapour mass fraction of the mixture, t_{dew} the dew point temperature of the mixture and F^{inv} the inverse of saturation line $F(t)$.

In the case of condensation a local energy balance for an element $dX\,dZ$ yields:

$$\dot{m}H_{lat} + \Theta_t \bar{h}_g(\bar{t}_g - t_i) = \bar{h}_{pl}(t_i - \bar{t}_l). \tag{15}$$

The interface temperature $t_i(X, Z)$ in this equation specifies $c_i(X, Z)$ since $c_i = F(t_i)$. The first term on the left-hand side of equation (15) represents the mass flux towards the condensate film where condensation takes place and the latent heat is liberated, while the second term represents the transported sensible heat, corrected for suction with the conventional Ackermann term.

The mass transport is caused by diffusion from mixture phase to condensate film. According to the classical film model this transport is described as [4]:

$$\dot{m} = \Theta_c \bar{g}_m \frac{\bar{c} - c_i}{1 - c_i}. \tag{16}$$

The determination of the mass transfer coefficient from mixture to condensate can be found in ref. [3].

The condensate drains along the plate surface under the action of gravity. On the right-hand side of equation (15) the heat transfer resistance of the condensate film is neglected. In ref. [3] it is derived that the contribution of a condensate film can be disregarded for pure vapour condensation because it is so thin. For partial condensation the mass flux towards the film is even smaller than for pure steam condensation, resulting in an even thinner film. This implies that the heat resistance of the film can safely be neglected in equation (15).

In equations (15) and (16) the classical film model correction factors Θ_c and Θ_t appear. That is to say, it is assumed *a priori* that fog is not formed in the mixture. Using the value of t_i obtained, and the associated value of c_i, the slope condition of refs. [5, 6] is used to examine whether the mixture is supersaturated near the wall:

$$\left.\frac{\mathrm{d}F}{\mathrm{d}t}\right|_{t_i} < \frac{\overline{Sh}}{\overline{Nu}_g} \frac{\Theta_c}{\Theta_t} \frac{\bar{c} - c_i}{\bar{t}_g - t_i}. \tag{17}$$

If this equation predicts supersaturation, the value of t_i obtained is not correct and has to be redetermined from equations (15) and (16) in which the fog film model correction factors $\Theta_{c,f}$ and $\Theta_{t,f}$, derived in refs. [5, 6], now have to be substituted. These correction factors are based on the saturation condition, which is the most ideal condition for fog formation. In reality supersaturation in the gas will always take place to some extent. Accordingly, actual heat and mass transfer have values in between those predicted by the conventional film model and the saturation fog film model.

With the value of t_i finally obtained the differential energy balances for the gas and liquid coolant sides and the mass balance for the gas side are derived. The heating of the liquid is described by equation (3) with associated boundary condition (4). In order to formulate the decrement in total mass flow rate, vapour mass fraction and mixture temperature the gas flow between the plates is considered in the following.

For a superheated mixture a differential mass balance between parallel plates yields:

$$\frac{\partial w_g}{\partial X} = -2LB\dot{m}. \tag{18}$$

The conservation of the non-condensables in the mixture leads to:

$$\frac{w_g(X, Z)}{w_{g,in}} = \frac{1 - c_{in}}{1 - \bar{c}(X, Z)}. \tag{19}$$

Equations (16), (18) and (19) are now combined into:

$$\frac{\partial \bar{c}}{\partial X} = -\frac{2\bar{g}_m LB}{w_{g,in}} \Theta_c \frac{\bar{c} - c_i}{1 - c_i} \frac{(1 - \bar{c})^2}{1 - c_{in}}, \tag{20}$$

with as boundary condition on $\bar{c}$:

$$\bar{c}(X = 0, Z) = c_{in}. \tag{21}$$

The variation of the gas temperature follows from the energy balance:

$$w_g c_{p,g} \frac{\partial \bar{t}_g}{\partial X} = -2LB\bar{h}_g \Theta_t (\bar{t}_g - t_i) + 2LB\dot{m}(\bar{t}_g - t_i) c_{p,v}. \tag{22}$$

With equations (2), (16), (20), (18) and (19) this equation is rewritten as:

$$\frac{\partial \bar{t}_g}{\partial X} = -\frac{2\bar{h}_g LB}{w_{g,in} c_{p,g}} \left(\Theta_t - \frac{\overline{Sh}}{Le_v \overline{Nu}_g} \Theta_c \frac{\bar{c} - c_i}{1 - c_i} \right) \times \frac{1 - \bar{c}}{1 - c_{in}} (\bar{t}_g - t_i) \tag{23}$$

with equation (6) as the boundary condition.

As soon as the mixture becomes saturated, so that $\bar{c}(X, Z) = F(\bar{t}_g(X, Z))$, and the the bulk properties are tending to supersaturation, fog is created in the bulk. The behaviour of the bulk properties is examined with equations (20) and (23) (refs. [5, 6]):

$$\frac{\mathrm{d}\bar{c}}{\mathrm{d}\bar{t}_g} = \frac{\overline{Sh}}{Le\,\overline{Nu}_g} \times \frac{\Theta_c \dfrac{\bar{c} - c_i}{1 - c_i} (1 - \bar{c})}{\left(\Theta_t - \dfrac{\overline{Sh}}{Le_v \overline{Nu}_g} \Theta_c \dfrac{\bar{c} - c_i}{1 - c_i} \right)(t_g - t_i)} < \left.\frac{\mathrm{d}F}{\mathrm{d}t}\right|_{\bar{t}_g}. \tag{24}$$

The differential mass and energy balances in case bulk fog is created are given by:

$$\frac{\partial \bar{c}}{\partial X} = -\frac{2\bar{g}_m LB}{w_{g,in}} \left(\Theta_c \frac{\bar{c} - c_i}{1 - c_i} + \frac{\bar{m}_f}{\bar{g}_m} \right) \frac{(1 - \bar{c})^2}{1 - c_{in}} \tag{25}$$

and

$$\frac{\partial \bar{t}_g}{\partial X} = -\frac{2\bar{h}_g LB}{w_{g,in} c_{p,g}} \left(\Theta_t - \frac{\overline{Sh}}{Le_v \overline{Nu}_g} \Theta_c \frac{\bar{c} - c_i}{1 - c_i} - \frac{H_{lat} \bar{m}_f}{\bar{h}_g (\bar{t}_g - t_i)} \right) \frac{1 - \bar{c}}{1 - c_{in}} (\bar{t}_g - t_i) \tag{26}$$

respectively. Applying equation (19), the effect of formed fog on the mass flow rate of the mixture is disregarded, because this amount is expected to be very small. For the same reason the influence of the droplets on the physical properties of the mixture is neglected. In the energy equation the bulk fog created appears as a heat source, and in the mass balance equation as a sink of matter. The bulk fog weakens the temperature drop and increases the fall of the vapour mass fraction. The amount of bulk fog is such that the mixture's bulk properties $\bar{c}$ and $\bar{t}_g$ follow the saturation line [5, 6]:

$$\overline{\dot{m}_f} = \left(\frac{\bar{h}_g(\bar{t}_g - t_i)}{H_{lat}}\right) \times \frac{\Theta_t \left.\frac{dF}{dt}\right|_{\bar{t}_g} - \frac{\overline{Sh}}{\overline{Nu}_g}\Theta_c \frac{\bar{c}-c_i}{1-c_i}\left(\frac{1}{Le_v}\left.\frac{dF}{dt}\right|_{\bar{t}_g} + \frac{1}{Le}\frac{1-\bar{c}}{\bar{t}_g - t_i}\right)}{\left.\frac{dF}{dt}\right|_{\bar{t}_g} + (1-\bar{c})\frac{Le_v}{Le}\frac{c_{p,v}}{H_{lat}}}. \quad (27)$$

In the case of fog formation in the film, the fog film model correction factors $\Theta_{c,f}$ and $\Theta_{t,f}$ are used in equations (15), (16), (20) and (22)–(27) instead of Θ_c and Θ_t, respectively. The path of the bulk properties is then examined with:

$$\frac{d\bar{c}}{d\bar{t}_g} = \frac{1}{Le}\frac{-\frac{1-\bar{c}}{1-c_i}\left.\frac{dF}{dt}\right|_{t_i}}{\frac{1}{Le_v}\frac{\bar{t}_g - t_i}{1-c_i}\left.\frac{dF}{dt}\right|_{t_i} - 1} < \left.\frac{dF}{dt}\right|_{\bar{t}_g} \quad (28)$$

instead of equation (24). Strictly speaking, equation (28) is a combination of equations (20) and (23), where Θ_c and Θ_t have been replaced by $\Theta_{c,f}$ and $\Theta_{t,f}$, respectively. In this paper both correction factors based on the asymptotic solution, as obtained in ref. [5], as well as the compounded correction factors of ref. [6] are employed, in order to investigate the differences in required calculational time and produced numerical results. The numerical solution procedure is described in detail in ref. [3]. In ref. [3] the computation of the mixing cup temperature, vapour mass fraction and fog content of the outflowing gas after the heat exchanger is given. These mean exit values are in general not identical to the ultimate exit values after mixing, owing to the crossflow principle and the possibility of multiple liquid passages. The mixture can therefore be in thermodynamic non-equilibrium. To attain a stable state, fog can be dissolved or extra created; these possible transformations of the bulk properties of the gas are also given in ref. [3].

PURE STEAM CONDENSATION

When (superheated) steam enters the duct heat transfer is highest since no diffusion resistance is built up next to the condensate film. For a superheated vapour besides the latent heat transfer, sensible heat transfer also contributes. This sensible heat transfer results in a decrease of mass transfer towards the plate and hence in the formation of condensate. Taking these effects into account, in this section the governing equations of the process are derived and solved. The procedure is illustrated in Fig. 4.

To examine whether condensation takes place, the local interface temperature is determined using equation (1), thus assuming condensation will not take place. If the calculated temperature is higher than the saturation temperature:

$$t_i \geqslant t_{sat} \quad (29)$$

the assumption of no condensation is correct. The differential energy balances (7) and (8) are then applicable. However, when equation (29) is not satisfied, condensation takes place and a local energy balance for an element $dX\,dZ$ yields equation (15), with t_i replaced by t_{sat}:

$$\dot{m}H_{lat} + \left[\frac{-\frac{\dot{m}c_{p,v}}{\bar{h}_g}}{e^{-\dot{m}c_{p,v}/\bar{h}_g} - 1}\right]\bar{h}_g(\bar{t}_g - t_{sat}) = \bar{h}_{pl}(t_{sat} - \bar{t}_l). \quad (30)$$

The first term on the left-hand side of this equation represents the latent heat liberated into the condensate film. The sensible heat flux is taken into account by the second term, which also contains the Ackermann correction factor for suction. A similar approach to superheated pure (benzene) vapour condensation was presented by Mizushina *et al.* [10].

The temperature rise of the liquid coolant in the channel plate is described by:

$$\frac{\partial \bar{t}_l}{\partial Z} = \frac{2\bar{h}_{pl}LB}{w_l c_{p,l}}(t_{sat} - \bar{t}_l) \quad (31)$$

with equation (4) as the boundary condition. As the pressure drop, compared with the absolute pressure, is very small in the gas channel, t_{sat} is approximately constant in the channel. When it is further assumed *a priori* that condensation takes place on the entire plate, equation (31) can be integrated and boundary condition (4) applied, yielding the liquid temperature in the plate:

$$\bar{t}_l(X, Z) = t_{l,in} + (t_{sat} - t_{l,in})(1 - e^{-(2\bar{h}_{pl}LB/w_l c_{p,l})Z}). \quad (32)$$

The maximum surface temperature $t_i(X = 0, Z = 1)$ is calculated by substitution of equations (32) and (6) into equation (1), producing:

$$t_i(X = 0, Z = 1) = t_{l,in} + \frac{\bar{h}_{tot}}{\bar{h}_{pl}}(t_{g,in} - t_{l,in}) + \frac{\bar{h}_{tot}}{\bar{h}_g}(t_{sat} - t_{l,in})(1 - e^{-2\bar{h}_{pl}LB/w_l c_{p,l}}). \quad (33)$$

If this temperature is smaller than t_{sat}, the assumption of entire plate condensation is correct. If this assumption is not correct, the coolant temperature is determined by numerical integration of equation (31) until the end of the condensation region of the plate is reached. For saturated steam, thus, $t_{g,in} = t_{sat}$, the surface temperature never exceeds the saturation temperature and hence equation (32) is true. In this case all heat taken up by the coolant stems from condensation. Hence, $t_{l,out}$ follows from equations (13) and

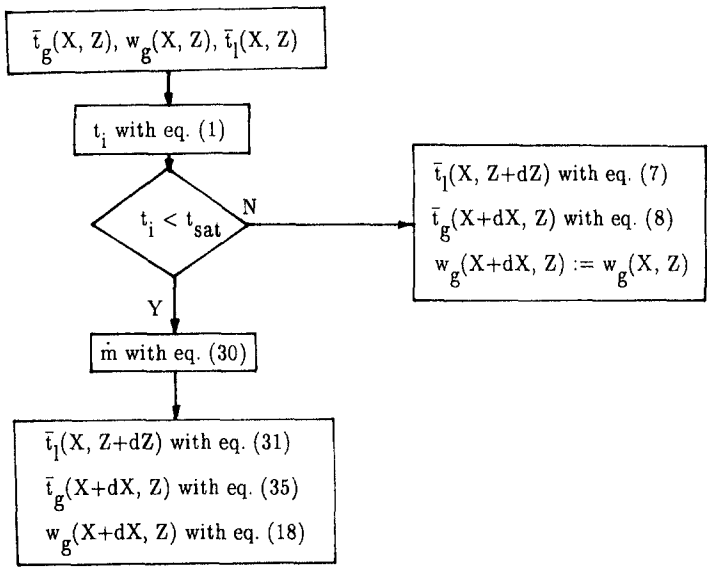

Fig. 4. Flow chart of calculational procedure for pure steam condensation.

(32), $t_{g,out} = t_{sat}$ and the exit steam mass flow rate from an overall mass balance.

In contrast to partial vapour condensation, the interface temperature is explicitly known in equation (30), namely $t_i = t_{sat}$, and need not to be determined iteratively. Instead of t_i the local mass flux $\dot{m}(X, Z)$ now has to be determined iteratively if the steam is superheated. Subsequently, with this mass flux the differential mass and energy balances at the gas (or steam) side are derived. At the gas side the decrease of the mass flow rate is described by equation (18), with the boundary condition on w_g:

$$w_g(X = 0, Z) = w_{g,in}. \tag{34}$$

The variation of gas bulk temperature is given by equation (22) with t_i replaced by t_{sat}. This equation is rewritten as:

$$\frac{\partial \bar{t}_g}{\partial X} = -\frac{2\bar{h}_g LB}{w_g c_{p,g}}(\Theta_t - \phi_t)(\bar{t}_g - t_{sat}) \tag{35}$$

with pertaining boundary condition (6). The numerical solution procedure of the governing equations is described in ref. [3].

COMPUTATIONAL RESULTS

Calculations on a PVDF heat exchanger with an effective length (L_{tot}) of 0.40 m and width of 0.384 m (corresponding to 96 parallel channel plates) have been carried out. The liquid (water) flow passes the channel plates twice, as depicted in Fig. 1. It flows through 48 plates from inlet to opposite headers, is collected there and mixed, and then flows through the 48 other plates to the exit of the heat exchanger. The initial water temperature is set equal to 19.5°C for the calculations. The entering gas, a mixture of air and water-vapour, has a temperature of 62°C and absolute pressure of 1.029 bar. The entry mass fraction of water-vapour, c_{in}, ranges from zero up to and including 0.142. These entry conditions are such that all aspects of the model treated here will occur, namely no condensation, condensation without fog formation and condensation and fog formation. Moreover, suction is small for small c_{in}, is larger for larger c_{in}, and is greatest for c_{in} equal to 0.142 (corresponding to a saturated mixture). The evaluation of the physical properties of both fluids is found in ref. [3].

In Fig. 5 the dimensionless exit temperatures of both fluids, defined as

$$\zeta = \frac{t - t_{l,in}}{t_{g,in} - t_{l,in}} \tag{36}$$

are depicted as a function of c_{in} for $NTU_g = 0.612$ and $NTU_l = 0.041$, and $NTU_g = 0.710$ and $NTU_l = 0.038$, and in Fig. 6 for $NTU_g = 1.001$ and $NTU_l = 0.039$, and $NTU_g = 1.270$ and $NTU_l = 0.036$. In both plots the dimensionless exit gas mass flow rate and fog mass flow are also depicted, both flows rendered dimensionless by means of the entry gas mass flow rate:

$$W = \frac{w}{w_{g,in}}. \tag{37}$$

For sake of clarity the dimensionless fog is multiplied by a factor of 10. The predictions of the compound fog film model (for all computations this model proved to produce identical results as the asymptotic fog film model) and the solutions of the classical film model (thus without fog), which are used as reference, are depicted in both figures.

One can see clearly in Figs. 5 and 6 that for small c_{in} no condensation takes place in the heat exchanger and consequently the exit mass flow rates equal the entry mass flow rates ($W_{g,out} = 1$). For $c_{in} \geqslant 0.017$ con-

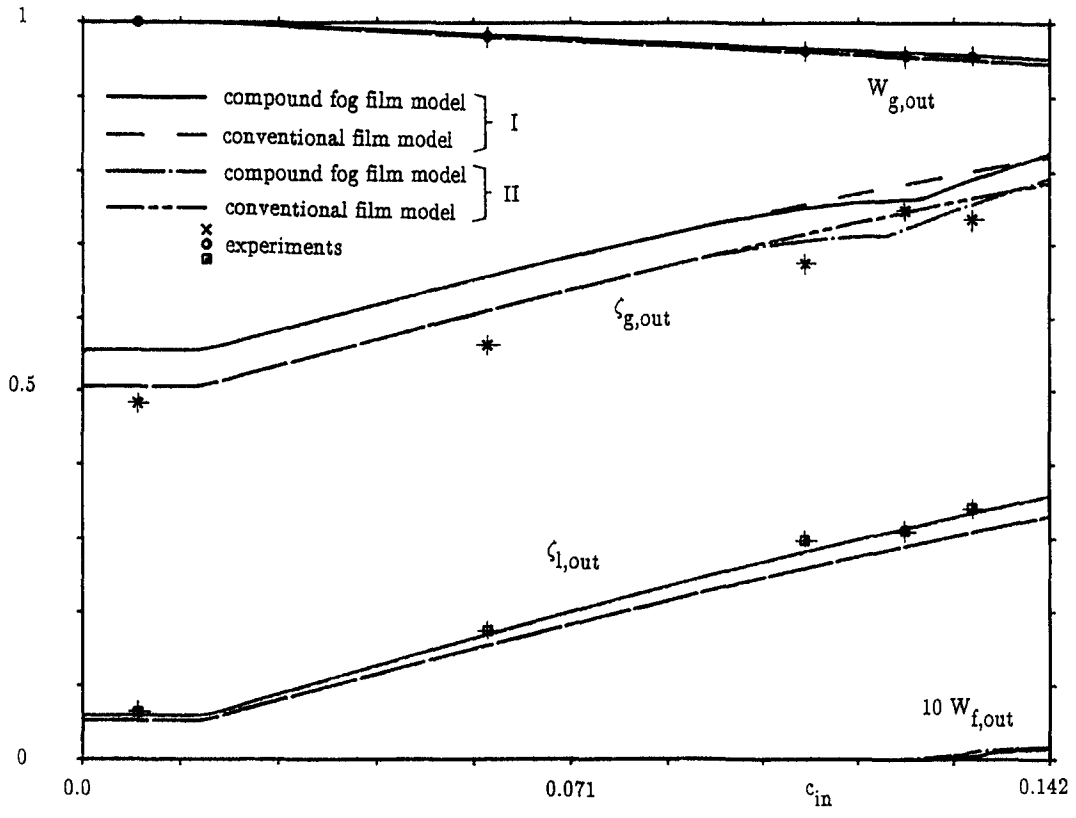

Fig. 5. Exit properties for $t_{l,in} = 19.5°C$, $t_{g,in} = 62°C$, $P_{tot} = 102\,900$ Pa, $NTU_g = 0.612$ and $NTU_l = 0.041$ (I), and $NTU_g = 0.710$ and $NTU_l = 0.038$ (II), according to the fog film model and conventional film model.

densation and liberation of latent heat commences in both figures, resulting in an exit temperature rise of both fluids and a decrease of the exit gas mass flow rate. For $c_{in} \geqslant 0.084$ and $c_{in} \geqslant 0.080$ in Figs. 5 and 6, respectively, fog formation near the wall appears to take place, indicated by a higher temperature drop at the gas side. As long as the bulk is superheated, formation of fog near the wall causes an enhanced sensible heat transfer; see ref. [6] for a graphical explanation.

For $c_{in} \geqslant 0.111$ and $c_{in} \geqslant 0.097$ in Figs. 5 and 6, respectively, fog is formed and latent heat is liberated in the bulk of the gas and the temperature fall is reduced. As the entry vapour mass fraction is close to the maximum (saturated) value, the bulk properties reach the saturation line sooner and the amount of bulk fog rises. Consequently, the exit gas temperature even exceeds the value provided by the conventional film model.

Figures 5 and 6 show that about one-third of the initial vapour present in the mixture condenses in the heat exchanger; the amount of (wall and droplet) condensed water is represented by the deviation of the dimensionless exit mass flow rate from unity. One can furthermore observe that the exit gas mass flow rate and related vapour mass fraction are predicted equally well by conventional and fog film models.

The numerical results indicate that the mass flow rate of wall condensed water is reduced by fog formation, since part of the condensed water, about 5%, has become fog. Both figures reveal that only a small part of the initial vapour flow leaves the heat exchanger as fog. Accordingly, the assumption that the droplets do not affect the physical properties of the gas appears to be correct *a posteriori*. Fog is, however, undesirable since it represents a yield loss and the formed droplets are difficult to remove. Additional computations with $t_{l,in} = 0°C$ furthermore revealed that in this common condition even 10% of the condensed water becomes fog, which is a substantial amount.

Further examination of Figs. 5 and 6 indicates that the exit coolant temperature is not reduced by fog formation. This would be expected; in refs. [5, 6] it was seen that the total (latent and sensible) heat flux towards a wall is not changed by fog formation. Both figures also illustrate that the fog and conventional film model deviate only in the prediction of exit gas temperature. For that matter, this deviation is very modest, typically 1°C. That is to say, the formation of fog and its effect on the process of heat and mass transfer will be hard to verify quantitatively, particularly if one realizes that a supersaturated mixture actually exhibits behaviour between the predictions of

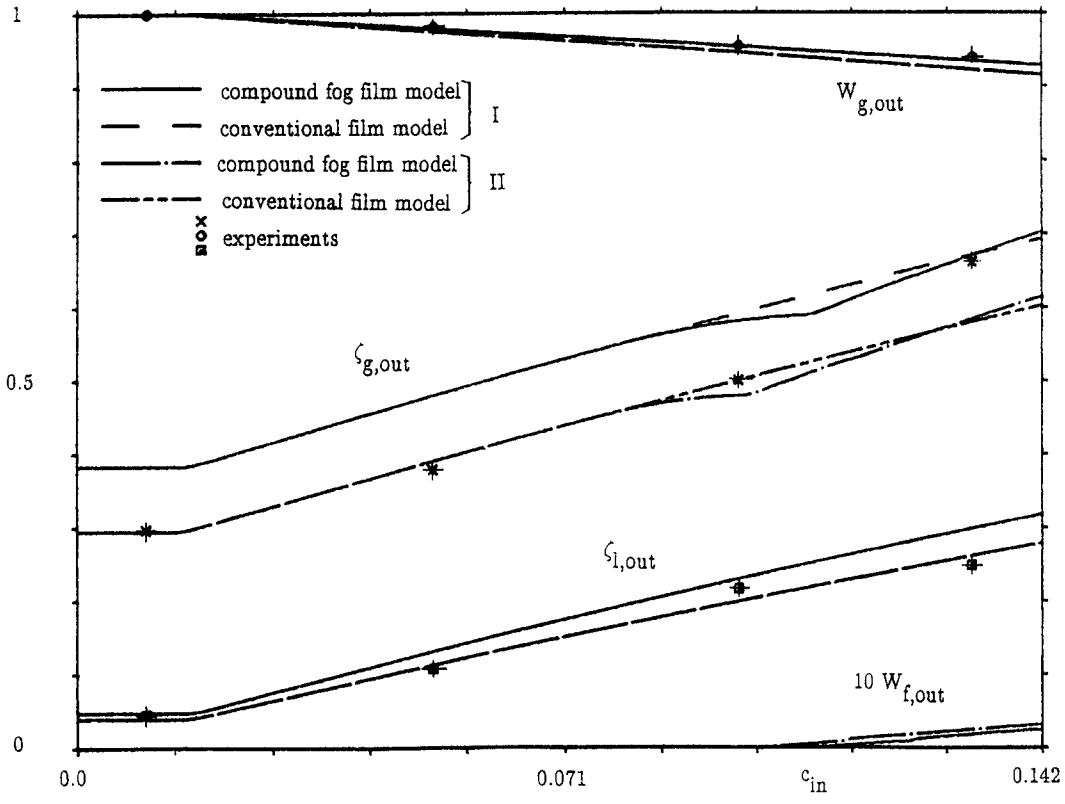

Fig. 6. Exit properties for $t_{l,in} = 19.5$ C, $t_{g,in} = 62$ C, $P_{tot} = 102\,900$ Pa, $NTU_g = 1.001$ and $NTU_l = 0.039$ (I), and $NTU_g = 1.270$ and $NTU_l = 0.036$ (II), according to the fog film model and conventional film model.

the conventional (i.e. perfect non-equilibrium) and fog film model, since the latter is based on the saturation condition (i.e. perfect equilibrium between vapour and droplet phase).

In Fig. 7 results of similar calculations are depicted for entry liquid and gas temperatures of 20 and 82°C, respectively, $P_{tot} = 101\,325$ Pa, $NTU_g = 0.656$ and $NTU_l = 0.042$, and $NTU_g = 0.741$ and $NTU_l = 0.038$, c_{in} ranging from zero up to and 0.388, which is the maximum and saturated vapour fraction. The figure shows the same trends as Figs. 5 and 6. The main difference is that the amount of transferred heat is larger, owing to the larger vapour fractions in the gas. Condensation starts for $c_{in} = 0.019$, which is a higher value than the values we have seen for $t_{g,in} = 62$°C in Figs. 5 and 6. This is due to the higher temperature of the gas and interface.

Fog is not formed in a layer next to the wall, which is attributed to the relation between temperature and vapour fraction in the film and the saturation line of water-vapour and air mixtures [5]. For higher vapour mass fractions and $Le_v < 1$ the bulk properties are also less (or not) directed into the supersaturated region and hence bulk fog is not likely to be formed. Accordingly, the solutions of the conventional and fog film model coincide.

The entry gas temperature pertaining to Fig. 8 is 100°C, $t_{l,in} = 20$°C, $P_{tot} = 101\,325$ Pa, $NTU_g = 0.621$ and $NTU_l = 0.042$, and $NTU_g = 0.742$ and $NTU_l = 0.038$. The largest c_{in} of this figure is unity, which corresponds physically to pure saturated steam entering (and leaving) the heat exchanger. Figure 8 indicates that condensation sets in for $c_{in} = 0.023$ and that for all cases no fog is formed. All mixtures are again sufficiently superheated, implying that the predictions of the fog film model and conventional film model coincide.

In order to indicate some characteristic features of the processes in the heat exchanger, the dimensionless interface temperature is determined for one group of the conditions of Fig. 8 ($NTU_g = 0.742$ and $NTU_l = 0.038$, marked by II). To this end, for a plate of the first pass, $\zeta_i(X = 0, Z = 0)$, $\zeta_i(1,0)$ and $\zeta_i(0,1)$ are determined, $\zeta_i(0,1)$ represents the maximum and $\zeta_i(1,0)$ the minimum temperature of gas-plate or gas-condensate film interface, respectively. It can be verified that $\zeta_i(0,1)$ depends only on NTU_l, $\zeta_i(1,0)$ on NTU_g and $\zeta_i(0,0)$ on neither of them.

For heat transfer without condensation these temperatures are known; $\zeta_i(0,0)$ is obtained by rewriting equation (1) and inserting equations (4), (6), (11) and (36):

$$\zeta_i(0,0) = \frac{\bar{h}_{tot}}{\bar{h}_{pl}}. \tag{38}$$

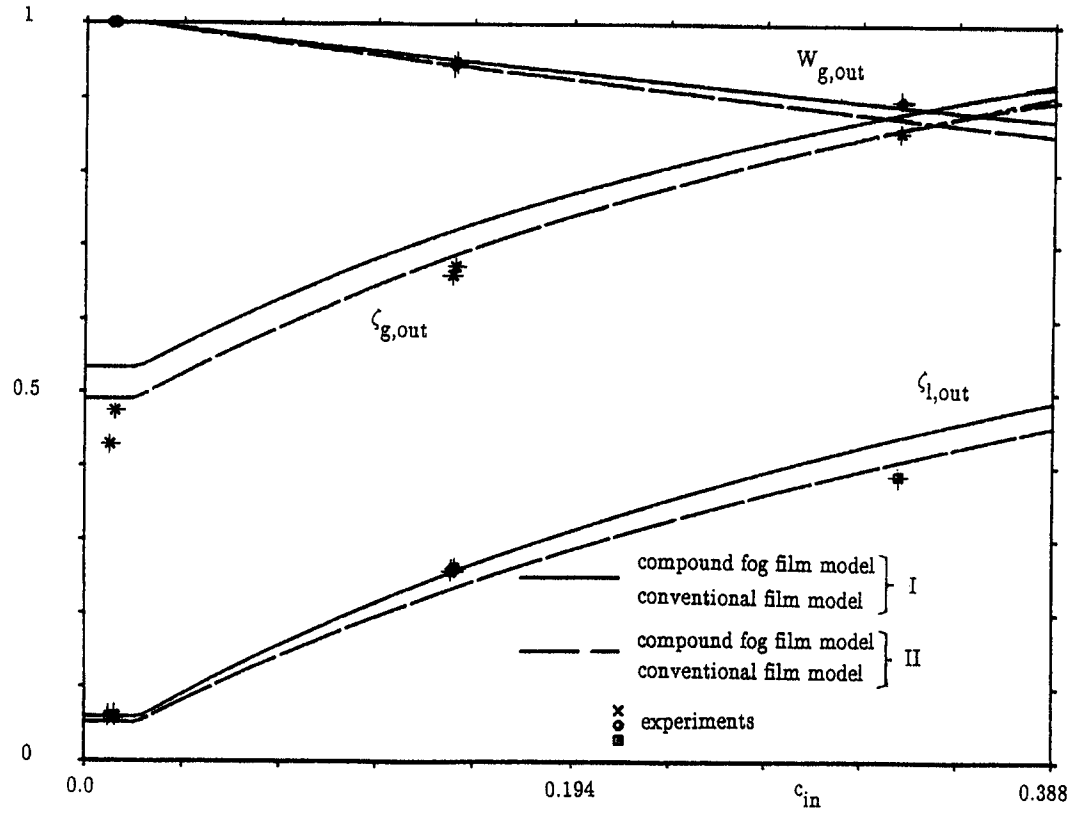

Fig. 7. Exit properties for $t_{l,in} = 20°C$, $t_{g,in} = 82°C$, $P_{tot} = 101\,325$ Pa, $NTU_g = 0.656$ and $NTU_l = 0.042$ (I), and $NTU_g = 0.741$ and $NTU_l = 0.038$ (II), according to the fog film model and conventional film model.

$\zeta_i(1,0)$ follows readily from equations (12) and (36), and $\zeta_i(0,1)$ is determined by solving equation (7) with application of equations (4) and (6), and substitution of the result in equation (36), yielding:

$$\zeta_i(0,1) = 1 - \frac{\bar{h}_{tot}}{\bar{h}_g} e^{-NTU_l}. \tag{39}$$

For $c_{in} = 1$, the pure steam condensation process, these three temperatures are also known, and $\zeta_i(X,Z)$ is uniform and equal to unity, since $t_{sat} = t_{g,in} = 100°C$.

In Fig. 9 $\zeta_i(0,0)$, $\zeta_i(0,1)$ and $\zeta_i(1,0)$ are drawn vs the initial vapour mass fraction. One can see the smooth transition from heat transfer without condensation, represented by horizontal lines, through partial condensation to pure steam condensation heat transfer. The onset of condensation is indicated by a sudden rise of ζ_i, at first in $(X,Z) = (1,0)$ and subsequently in (0,0) and (0,1). In order to assess the uniformness of ζ_i over the condensate surface, the ratios $\zeta_i(1,0)/\zeta_i(0,0)$ and $\zeta_i(0,0)/\zeta_i(0,1)$ are also depicted in Fig. 9. These lines indicate that the interface temperature is not uniform in both the direction of X and Z; the interface temperature ratios differ significantly from unity, except for c_{in} close to unity. Despite the frequent assumption in conventional condenser analysis of uniform condensate interface temperature, here this temperature depends substantially on the coordinates X and Z. Or, in other words, the processes and pertaining models are essentially two-dimensional.

The accuracy of the numerical procedures has been assessed by varying the number of discretization points and considering their effect on exit values. These computations revealed that for 15×15 points the numerical error is less than 1%. For the examined heat exchanger with two passes this grid corresponds to a computational time of 60 s on an IBM AT PC for partial condensation and fog formation, 30 s for partial condensation and 15 s for pure vapour condensation. These values serve the objective of the present investigation very well. All computations disclosed that the predictions of the approximate fog film model of ref. [5] are practically identical to those of the compound fog film model of ref. [6], but that the computational time of the former is twice as long.

EXPERIMENTS

The theoretical predictions of the previous section are now compared with some experiments performed with a heat exchanger placed in a low speed wind tunnel (Fig. 10). The main features of the test rig can be found in ref. [3].

The experimental results depicted in Fig. 5, and the uncertainties in both NTUs, as derived in ref. [3],

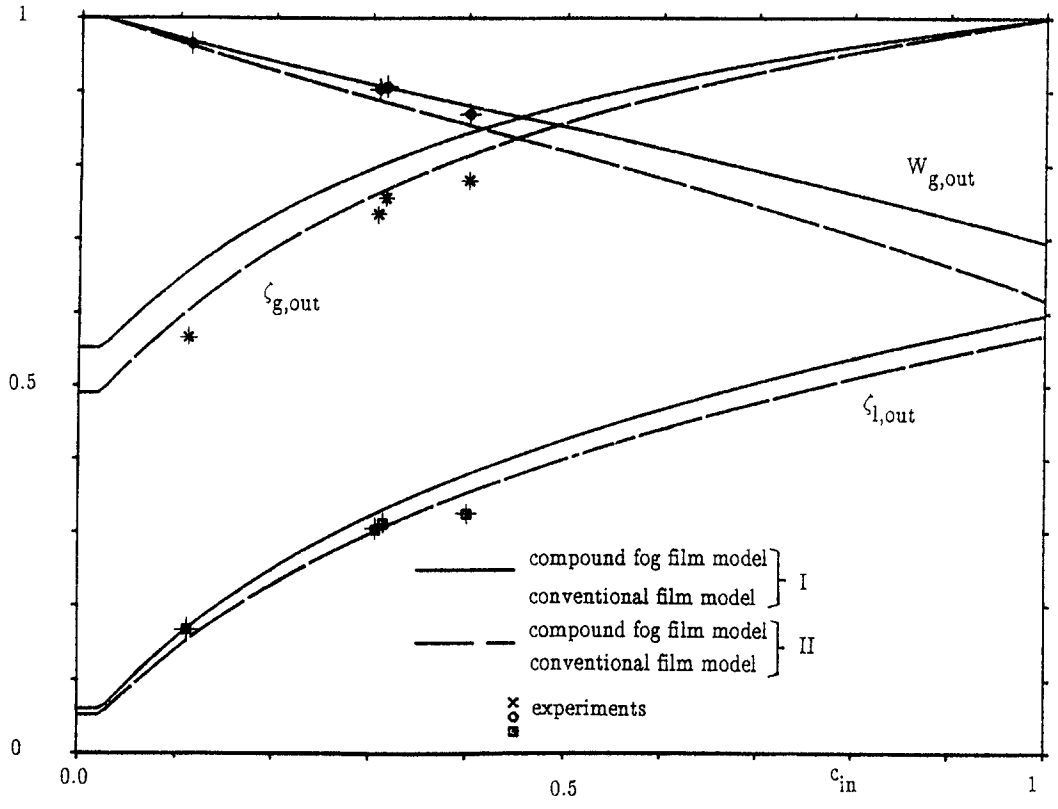

Fig. 8. Exit properties for $t_{l,in} = 20$ C, $t_{g,in} = 100$ C, $P_{tot} = 101\,325$ Pa, $NTU_g = 0.621$ and $NTU_l = 0.042$ (I), and $NTU_g = 0.742$ and $NTU_l = 0.038$ (II), according to the fog film model and conventional film model.

indicate that their NTU_l ranges from 0.038 to 0.041 and NTU_g from 0.612 to 0.710. These values imply that the experimental dimensionless exit values should be located between the two theoretical situations depicted in Fig. 5. Both cases represent the most extreme conditions: the smallest liquid flow and largest gas flow (marked by I); and the largest liquid flow in combination with the smallest gas flow (II). For the same reason the experimental results, selected for Figs. 6–8, have to lie between the depicted theoretical solutions as well. In ref. [3] all experimental results are documented, and supplied with an overall energy balance to assess the accuracy of the measurements. The vertical and horizontal bars in Figs. 5–8 are the ranges of uncertainty in the primary measurements of temperature, relative humidity, condensate weight and time.

The liquid exit temperatures suggest that the theoretical predictions overestimate the true heat and mass transfer for large condensation rates. This overprediction of heat and mass transfer is attributed to the actual heat resistance of the condensed water. In this analysis this resistance has been neglected and will be the subject of further study. During the condensation experiments it was observed that, contrary to the assumptions of the model, the water condensed dropwise on the PVDF channel plates, sometimes even forming bridges between adjacent parallel walls. Figures 5–8 also show the trend that the theoretical mass transfer rates overestimate the true mass fluxes, while the true sensible heat transfer appears to be better than theoretically expected.

In the previous section it was explained that it is difficult to detect quantitatively the effect of fog formation on exit properties and that it can be detected qualitatively only. To this end, a 300 W light was used to illuminate the gas flow in the glass chambers before and after the heat exchanger, and detect the threshold entry vapour mass fraction that results in fog formation. Fog is first observed in the gas that leaves the plates of the first liquid pass (more specifically: where the cold liquid enters the plates) and subsequently, on increasing c_{in}, downstream of the plates of the second pass. The gas flows are separated by a plate of 0.2 m to avoid direct contact and mixing of both flows. To promote fog formation and avoid supersaturation as much as possible, extra nuclei are added to the gas flow. These nuclei are generated by glowing saw dust at the entrance of the wind tunnel. A typical glowing rate is 0.3 kg saw dust per hour, while the total gas mass flow rate at the entrance of the tunnel (corresponding to 96 $w_{g,in}$) varies from 0.2 to 0.5 kg s^{-1}. In Tables 1 and 2 the experimentally determined bounding c_{in} (for each pass) of no fog/fog for the

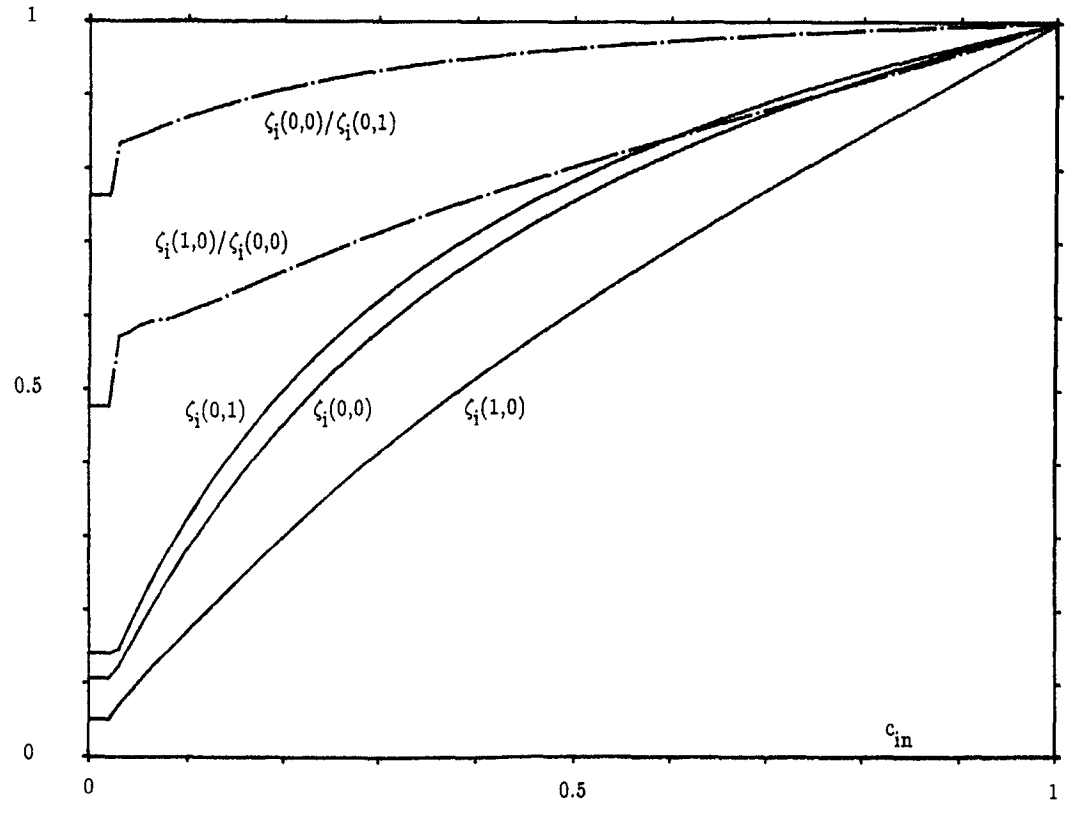

Fig. 9. Interface temperatures for $t_{l,in} = 20°C$, $t_{g,in} = 100°C$, $P_{tot} = 101\ 325$ Pa, $NTU_g = 0.742$ and $NTU_l = 0.038$, according to the fog and conventional film model.

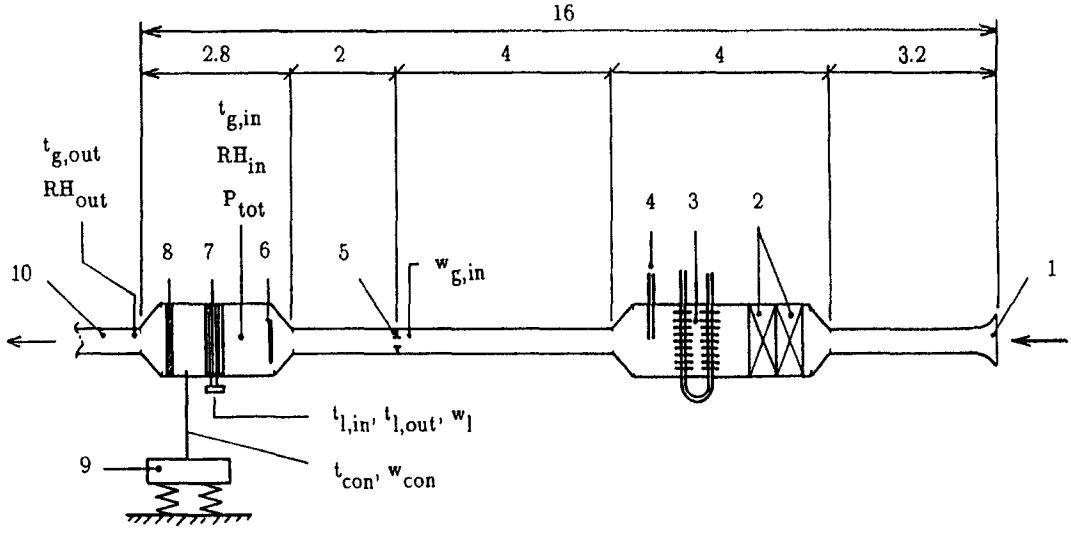

Fig. 10. Experimental apparatus (sizes in metres).

underlying conditions of Figs. 5 and 6, respectively, are listed. It is found that the extra nuclei are needed to create visible fog in the vicinity of the critical c_{in}. For c_{in} values that significantly exceed this threshold value nuclei are not needed.

In both tables the theoretical predictions for the onset of film and bulk fog are also included. These tables show that fog formation starts for a lower c_{in} if NTU_g is relatively large (which is to say a small gas flow) and NTU_l is small (large liquid flow). The results indicate that the experimental threshold c_{in} corresponds to the theoretical boundaries for developing bulk fog. It is also possible of course that film fog is observed and that the difference in c_{in} (about 0.02)

Table 1. Theoretical and experimental threshold entry vapour mass fractions, c_{in}, for film and/or bulk fog formation

	First pass		Second pass	
Theoretical	Film	Bulk	Film	Bulk
$NTU_g = 0.612$, $NTU_l = 0.041$	0.084	0.111	0.104	0.127
$NTU_g = 0.710$, $NTU_l = 0.038$	0.081	0.105	0.100	0.123
Experimental				
Fog observation	0.106		0.121	

Table 2. Theoretical and experimental threshold entry vapour mass fractions, c_{in}, for film and/or bulk fog formation

	First pass		Second pass	
Theoretical	Film	Bulk	Film	Bulk
$NTU_g = 1.001$, $NTU_l = 0.039$	0.078	0.097	0.094	0.115
$NTU_g = 1.270$, $NTU_l = 0.036$	0.076	0.088	0.087	0.104
Experimental				
Fog observation	0.097		0.111	

can be attributed to supersaturation. However, in the temperature and saturation mass fraction regions considered ($20 \leqslant t \leqslant 62°C$, $0.014 \leqslant F(t) \leqslant 0.142$) a vapour supersaturation of 0.02 corresponds to a temperature supercooling of about 6.5°C. Such a supercooling level is not likely since Brouwers [11] found visible fog formation to occur if supercooling exceeds 1–2°C. Accordingly, the experimental and theoretical results are considered as an indication for the correctness of the application of the fog film model to channel flow.

The main physical feature of the suggested procedures is the distinction made between film and bulk fog. Created film fog is neglected as long as the bulk properties are superheated, legitimized by the thinness of the film in which mass and heat are transferred. This approach is allowed for turbulent and developing laminar channel flow. In either of these situations one can actually speak of a bulk and a thin film next to the wall where heat and mass are transferred. The gas entering and flowing between the channel plates never attains a parabolic velocity profile as $Re_g > 500$ (the minimum and maximum NTU_g and NTU_l of Tables 1 and 2 correspond to gas flow Reynolds numbers ranging from 520 to 1210 and liquid flow Reynolds numbers ranging from 250 to 300, respectively). Following Ward-Smith [12], fully developed flow is attained for:

$$\frac{B_{tot}}{D_{h,g}} > 0.04\, Re_g. \tag{40}$$

So for $Re_g > 500$ the developing length takes at least 20 $D_{h,g}$, while the length of the gas channel B_{tot} approximates 19 $D_{h,g}$, see Fig. 2. Moreover, the droplets on the plates prevent a smooth development of laminar flow and promote transverse mixing in the gas. All these features of the flow between the plates might be the reason why the agreement with the experimental observations is so good.

The suggested fog film model approach to channel flow is less suited for fully developed laminar channel flow of gas mixtures (which is rarely found in engineering applications). Hayashi *et al.* [13] observed a superheated core in the presence of a fogging layer next to the wall. These regions were observed in mixtures of wall condensing water-vapour and air flowing between parallel plates.

CONCLUDING REMARKS

Two-dimensional crossflow models are presented that describe heat and mass transfer in gas–liquid plastic compact heat exchangers. These models involve heat transfer without condensation, pure steam condensation, and condensation and fog formation in the presence of non-condensables. Both the conventional film model and the fog film models of refs. [5, 6] are employed to predict heat and mass transfer.

Numerous heat transfer computations of various air–water-vapour mixtures revealed that the compound fog film model of ref. [6] produces identical results to those of the asymptotic fog film model of ref. [5], but that the required computational time of the latter is twice as long. The entire investigation further revealed that the governing equations of all physical situations can be solved within a very short calculational time. Hence the presented models and solution procedures are well executable on a (portable) PC.

In the case of condensation the results indicate that a considerable part of the initial vapour flow remains as condensate in the heat exchanger; this is due to the compact geometry of channel plates and heat exchanger. The amount of bulk fog formed is found to be very modest for the selected conditions and can

be verified qualitatively only. Moreover, the heating up of the primary liquid is not affected by fog formation. A typical result is that, except for small air fractions, the interface temperature of the condensate film is not uniform and depends on the location in the heat exchanger.

The theoretical predictions are compared with experimental data obtained with a PVDF heat exchanger. The entry liquid temperature $t_{l,in}$ is about 20°C and $t_{g,in}$ varies from 60 to 100°C; the entry vapour mass fraction c_{in} ranges from zero up to 0.40. For $t_{g,in} \cong 80$°C and $t_{g,in} \cong 100$°C, fog formation is not predicted and not observed. For $t_{g,in} \cong 60$°C fog formation is predicted and observed. The observations suggest the correctness of the proposed application of the fog film model to channel flow.

The condensation model issues from the approximation that the effect of the water condensate film on heat transfer can be disregarded so that the process of heat and mass transfer is driven by the difference between the liquid temperature in the plate and the gas–condensate interface temperature. Hence, it is not affected by condensate production and flow along the plate. The concurrent and countercurrent condensation experiments illustrate that this simplification results in a slight overestimation of the heat exchanger's performance, in particular when c_{in} and—dropwise—condensation rate rise (it should be noted that this dropwise condensation is in contrast to the filmwise condensation that was assumed). However, for a heat exchanger operating in crosscurrent condensation and concurrent gas flow the effect of the condensate is expected to be low. The analysis of the condensation of water on PVDF plates forms the subject of a future study [14].

If an order of magnitude analysis for vapour other than water also yields the conclusion that the effect of the condensate is small, the model presented can be applied directly to the condensation of that particular vapour. Moreover, although attention was focused on plastic heat exchangers, the analysis can very well form the basis for modelling the heat transfer in other types of crossflow heat exchangers. One needs only to assess the condensate formation and its heat resistance, and apply the Nusselt number correlations pertaining to the geometry of the heat exchanger and the prevailing flow conditions.

Acknowledgements—The authors wish to thank Messrs. H. P. Korstanje and G. Vegt for their support of this work and the management of Akzo Nobel Central Research Arnhem for their permission to publish this paper. The experimental assistance of Messrs. J. M. W. M. Schoonen, S. Beekmans and P. Maclean is greatly acknowledged.

REFERENCES

1. A. C. Bannwart, Etude théoretique et expérimentale de la condensation d'une vapeur en présence d'incondensables, Thèse de Doctorat, Institut National Polytechnique de Grenoble, Grenoble (1988).
2. A. C. Bannwart and A. Bontemps, Condensation of a vapour with incondensables: an improved gas phase film model accounting for the effect of mass transfer on film thicknesses, *Int. J. Heat Mass Transfer* **33,** 1465–1474 (1990).
3. H. J. H. Brouwers, Film models for transport phenomena with fog formation, with application to plastic heat exchangers and condensers, Ph.D. Thesis, Eindhoven University of Technology, Eindhoven (1990).
4. H. J. H. Brouwers and A. K. Chesters, Film models for transport phenomena with fog formation: the classical film model, *Int. J. Heat Mass Transfer* **35,** 1–11; 2067 (1992).
5. H. J. H. Brouwers, Film models for transport phenomena with fog formation: the fog film model, *Int. J. Heat Mass Transfer* **35,** 13–28 (1992).
6. H. J. H. Brouwers, A film model for heat and mass transfer with fog formation, *Chem. Engng Sci.* **47,** 3023–3036 (1992).
7. W. Nusselt, Der Wärmeübergang im Kreuzstrom, *Z. Ver. dt. Ing.* **55,** 2021–2024 (1911).
8. B. S. Baclic and P. J. Heggs, On the search for new solutions of the single-pass crossflow heat exchanger problem, *Int. J. Heat Mass Transfer* **28,** 1965–1976 (1985).
9. J. L. Mason, Heat transfer in crossflow, *Proceedings Second U.S. National Congress of Applied Mechanics*, pp. 801–803, ASME, New York (1955).
10. T. Mizushina, R. Ito, S. Yamashita and H. Kamimura, Film condensation of a pure superheated vapor inside a vertical tube, *Int. Chem. Engng* **18,** 672–679 (1978).
11. H. J. H. Brouwers, An improved tangency condition for fog formation in cooler-condensers, *Int. J. Heat Mass Transfer* **34,** 2387–2394 (1991).
12. A. J. Ward-Smith, *Internal Fluid Flow*. Clarendon Press, Oxford (1980).
13. Y. Hayashi, A. Takimoto and Y. Yamamoto, Heat and mass transfer with mist formation in a laminar duct flow, *Heat Transfer—Jap. Res.* **10,** 37–51 (1978).
14. C. W. M. Van der Geld and H. J. H. Brouwers, The mean condensate heat resistance of dropwise condensation with flowing, inert gases, accepted for publication in *Wäime- und Stoffübertragung/Thermo- and Fluid Dynamics*.